Science Advances
AAAS

advances.sciencemag.org/cgi/content/full/5/8/eaav7172/DC1

Supplementary Materials for

The role of aseismic slip in hydraulic fracturing–induced seismicity

Thomas S. Eyre*, David W. Eaton, Dmitry I. Garagash, Megan Zecevic, Marco Venieri, Ronald Weir, Donald C. Lawton

*Corresponding author. Email: thomas.eyre@ucalgary.ca

Published 28 August 2019, *Sci. Adv.* **5**, eaav7172 (2019)
DOI: 10.1126/sciadv.aav7172

This PDF file includes:

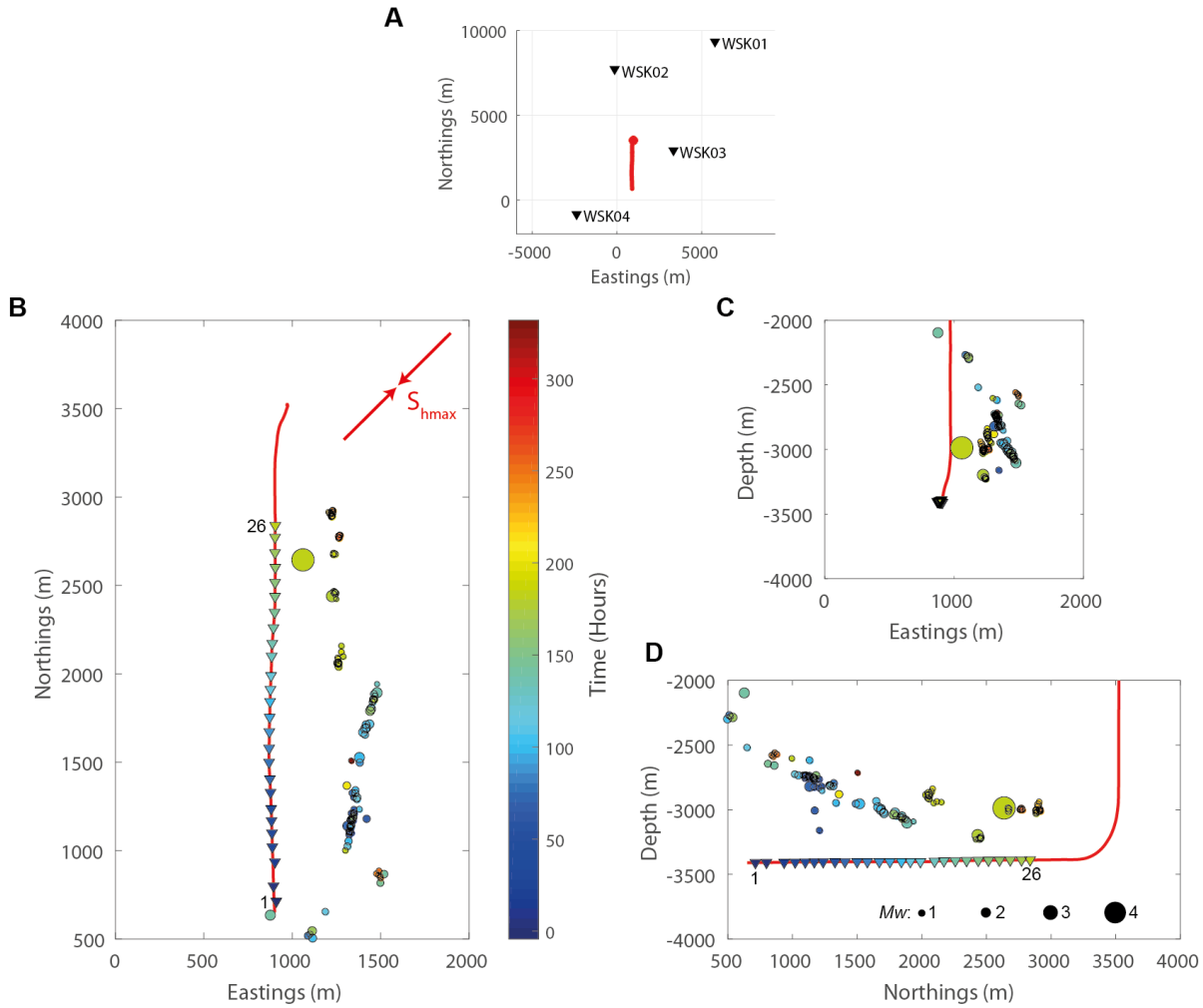

Fig. S1. Broadband seismic event locations. (**A**) The broadband seismic network used to obtain the data. Triangles represent the broadband stations, and the line shows the treatment well, with wellhead denoted by the star. (**B**) Map view, (**C**) west-east cross-section, and (**D**) south-north cross-section of the estimated seismic event locations, colored by time. Marker size is exponentially scaled by magnitude so that the largest events can be identified (scale in (D)). Stages are shown as numbered black outlined triangles colored by time.

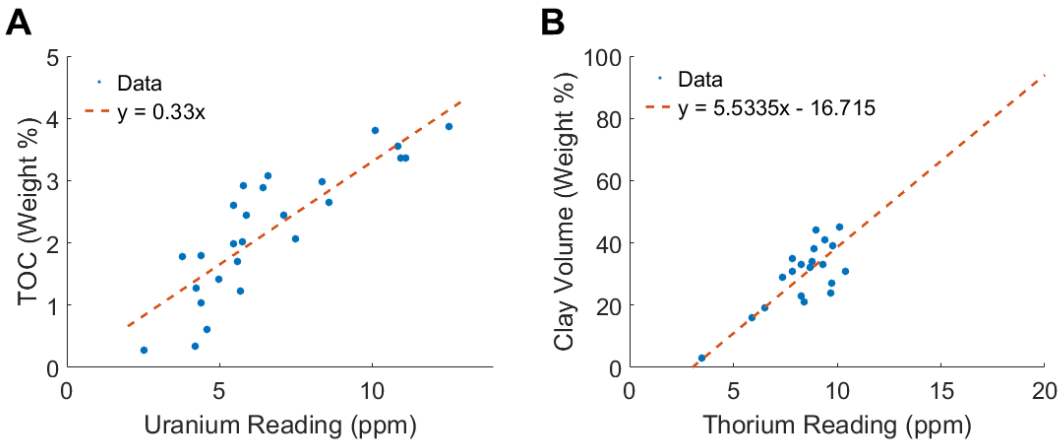

Fig. S2. Uranium-to-TOC and Thorium-to-clay correlations for a well ~17 km SE of the treatment wellpad. (**A**) Plot of uranium versus TOC and (**B**) plot of thorium versus clay volume. The lines of best fit are used to create conversion factors to obtain TOC from uranium readings and clay volume from thorium readings.

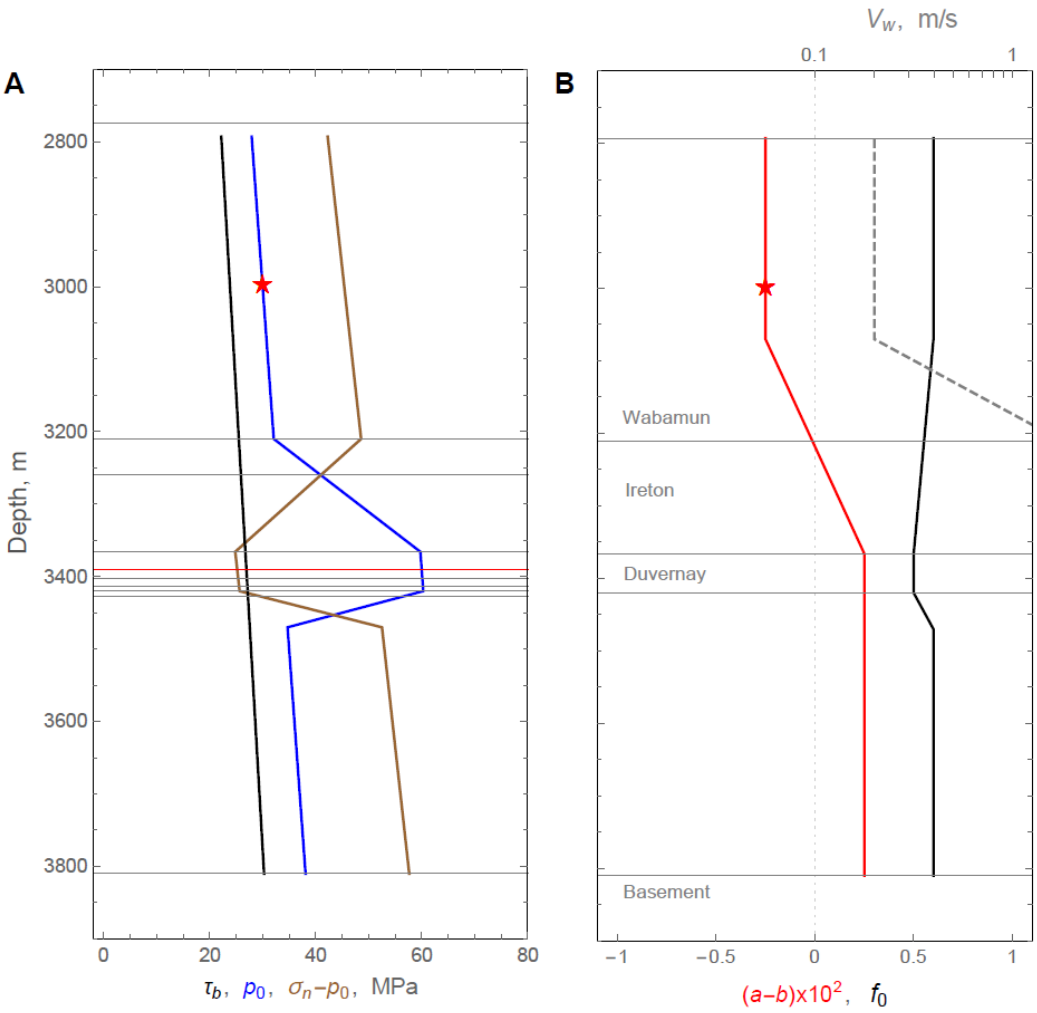

Fig. S3. Model of a vertical strike-slip fault intersecting the Duvernay. (**A**) Distribution of ambient overpressure (blue), shear (black) and effective normal (brown) stress resolved on a vertical fault at 45° to maximum in-situ stress. (**B**) Distribution of the low-velocity rate-state friction parameters (nominal friction f_0 at 1 micron/s slip rate and the steady-state friction slip-rate sensitivity parameter $a\text{-}b = df_{LV}/d\ \ln V$), with "stable" friction in the Duvernay (values based on the measured average TOC + clay content and frictional calibration of (*19*)), "unstable" low-velocity friction in the carbonate (Wabamun/Winterburn) unit (based on (*42*,*59*)), and a taper in-between. Distribution of the threshold velocity V_w for the onset of flash heating (high slip velocity weakening) of carbonate from the minimum value of 0.2 m/s (fig. S6) in the updip part of Wabamun, increasing exponentially with depth (rendering downdip parts of the fault including Ireton and Duvernay not susceptible to high velocity weakening).

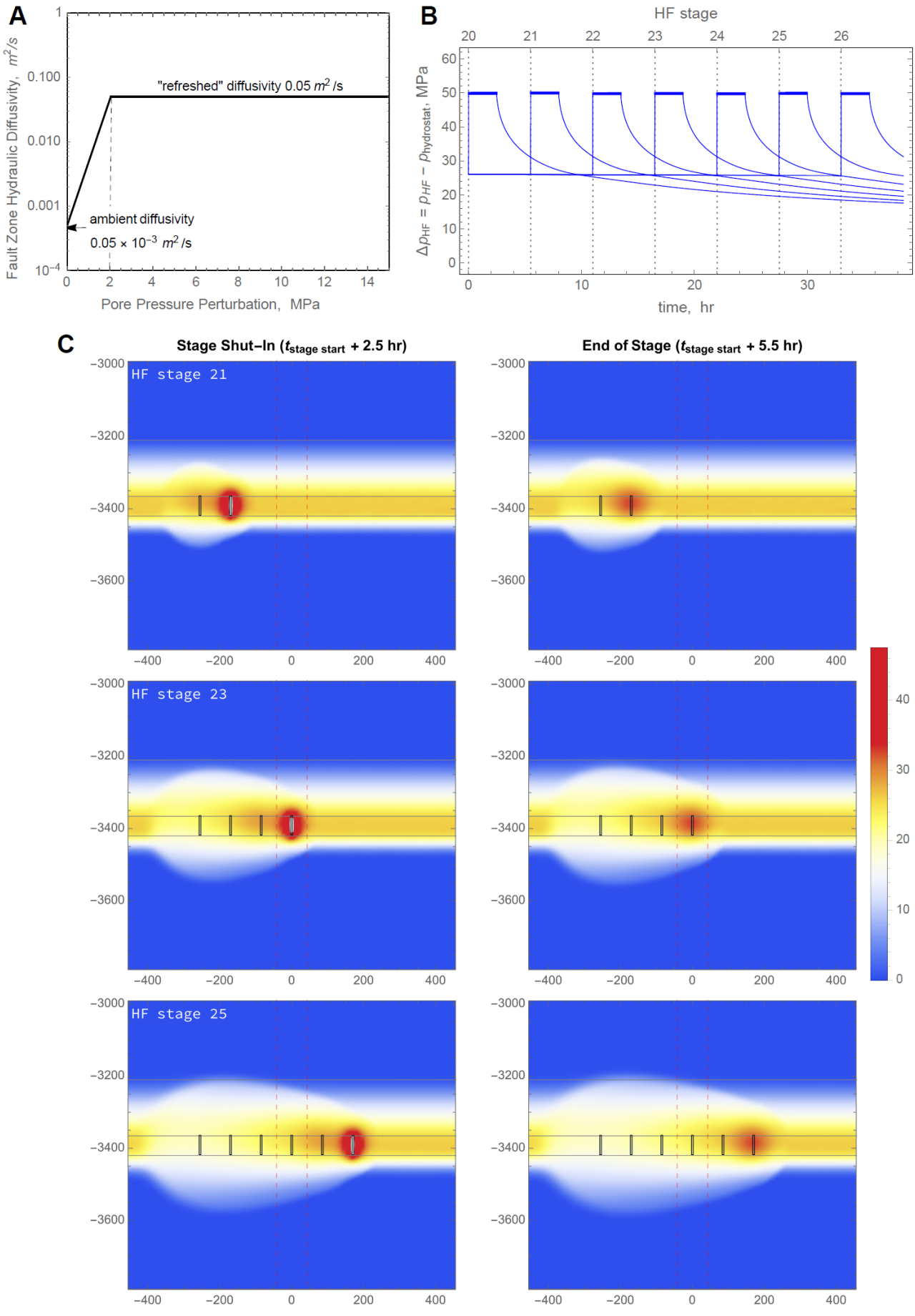
A
Fault Zone Hydraulic Diffusivity, m^2/s
1
0.100
0.010
0.001
10^{-4}
"refreshed" diffusivity 0.05 m^2 /s
ambient diffusivity
0.05 × 10^{-3} m^2 /s
0
2
4
6
8
10
12
14
Pore Pressure Perturbation, MPa
B
HF stage
20
21
22
23
24
25
26
$\Delta p_{HF} = p_{HF} - p_{hydrostat}$, MPa
60
50
40
30
20
10
0
0
10
20
30
time, hr
C
Stage Shut-In ($t_{stage\ start}$ + 2.5 hr)
End of Stage ($t_{stage\ start}$ + 5.5 hr)
HF stage 21
HF stage 23
HF stage 25
−3000
−3200
−3400
−3600
−400
−200
0
200
400
40
30
20
10
0

Fig. S4. Modeling of pore pressure diffusion along a vertical fault intersected by hydraulic fracture stages within the Duvernay formation. (**A**) Fault zone hydraulic diffusivity. The long-term low value of the fault zone hydraulic diffusivity is refreshed by pore pressure perturbation. (**B**) Overpressure at the intersections of the fault with stages (20 - 26) separated by 5.5 hours in time and by 85 m along the fault strike. The maximum value is prescribed during the stage fluid pumping at the average ISIP value of 50 MPa recorded for the treatment well (Table S1). During the shut-in for each stage, the pressure spontaneously dissipates as no fluid exchange between the hydraulic fracture and the fault is assumed. Pore pressure diffusion is slow enough not to alter the pore pressure at a given stage-fault intersection prior to its pumping. (**C**) Snapshots of 2D diffusion of pore pressure in excess of hydrostatic (MPa) along the fault. Stages 20-26 (black thin rectangles within the Duvernay formation) are modeled, while stages 21, 23, and 25 (the stage shut-in and the end of stage) are shown. The 1D ambient overpressure structure (fig. S3a) is evident ahead of the progression of the hydraulic fracture stages. The long-term low fault zone hydraulic diffusivity is refreshed by propagating hydraulic fracture overpressure. Fault section centered on stage 23 (marked by vertical red dashed lines) is used for the pore pressure along-strike average which is then used in the 1D (along-dip) modeling of fault slip (see Fig. 5d).

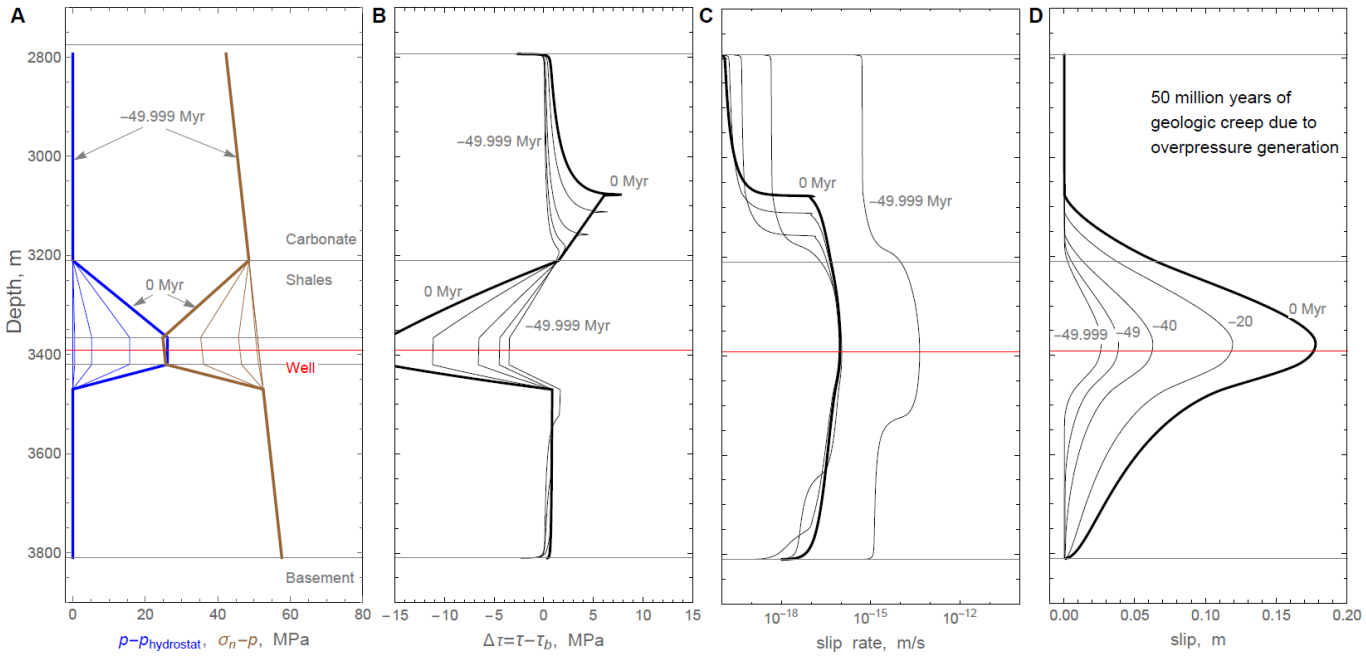

Fig. S5. Geologic creep of a vertical strike-slip fault intersecting the Duvernay over a 50-Ma window of reservoir pore overpressure generation. (**A**) Change in pore pressure (blue) and effective normal stress (brown). (**B**) Change in shear stress $\Delta\tau$. (**C**) Slip rate. (**D**) Slip. All are plotted against depth for different time steps, with treatment well depth shown as a red line.

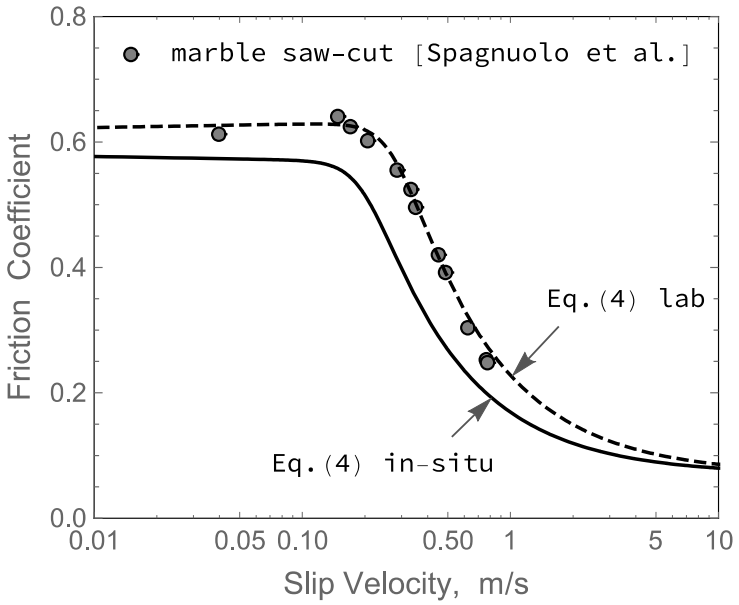

Fig. S6. Steady-state friction of carbonate-bearing fault accounting for flash heating at asperity contacts (*37*) modelled by Eq. (4). Lab data on friction of Carrara marble saw-cut from (*37*) and theoretical Eq. 4 with the fully flash-heated friction value f_w = 0.07, the threshold weakening slip velocity V_w = 0.28 m/s (lab), 0.2 m/s (in situ), and the low-velocity friction velocity dependence coefficient a-b = + 0.0025 (lab), - 0.0025 (in situ). The values of other frictional parameters in Eqs. 3 and 4 are given in the text.

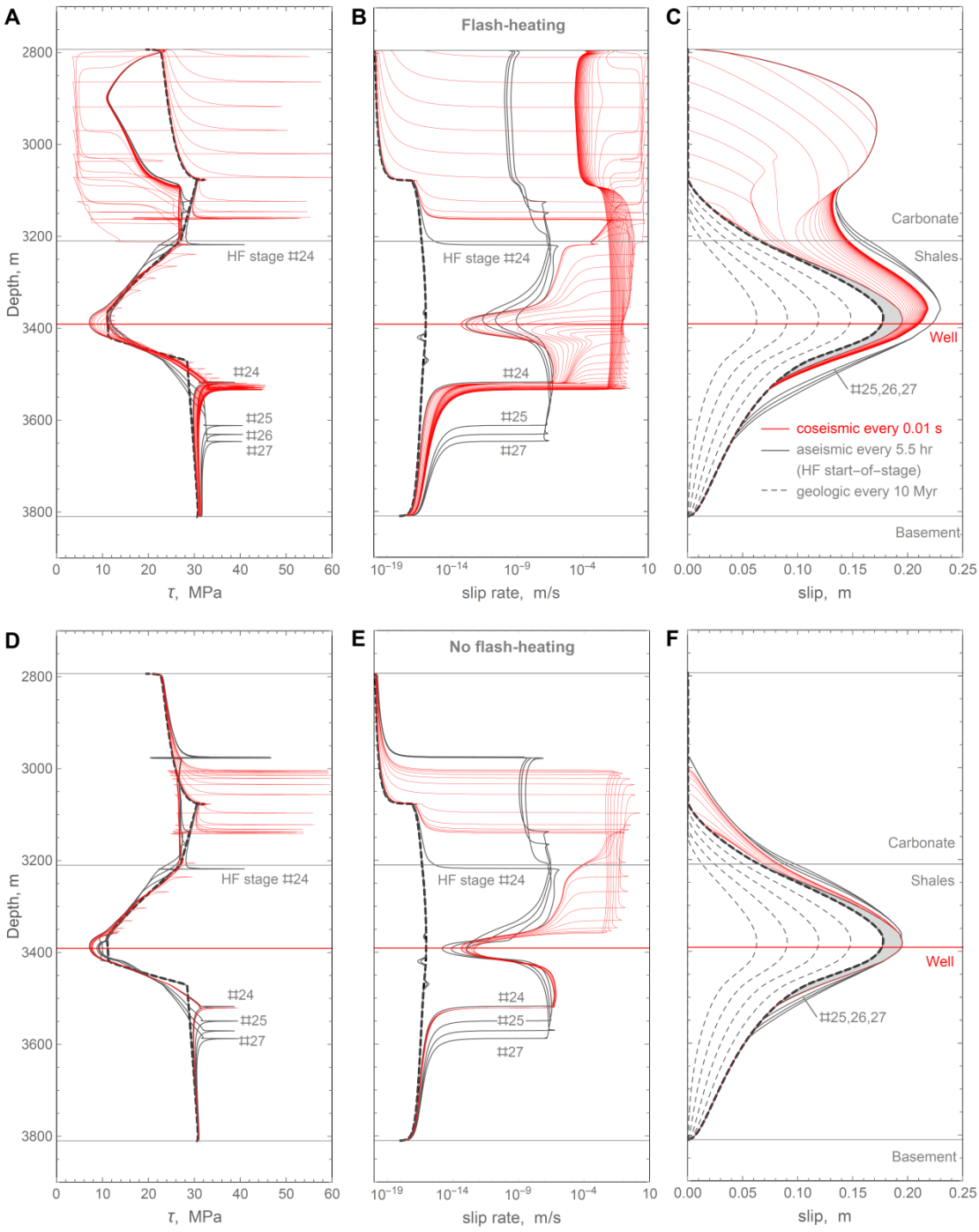

Fig. S7. Evolution of shear stress, slip rate, and slip along the fault induced by hydraulic fracturing (encapsulated in the evolution of the fault effective stress normal in Fig. 5b) shown by continuous gray lines every 5.5 hours starting from stage 23 (accelerated creep), and by red continuous lines every 0.01 s (coseismic slip). Thick black dashed line shows the ambient (prior to hydraulic fracture stimulation) state. (**A**) to (**C**) show the solution with flash-heating (strong dynamic friction weakening, as in Fig. 5), while (**D**) to (**F**) show the solution without flash heating. Note the gray stress peaks marking the fronts of the accelerated creep as it spreads both up-dip and down-dip through shales, outpacing the pore-pressure diffusion front in Fig. 5b. The rupture nucleates after the up-dip creep front impinges on the seismogenic carbonate unit (early stage 24). Stage #27 = end of stage 26.

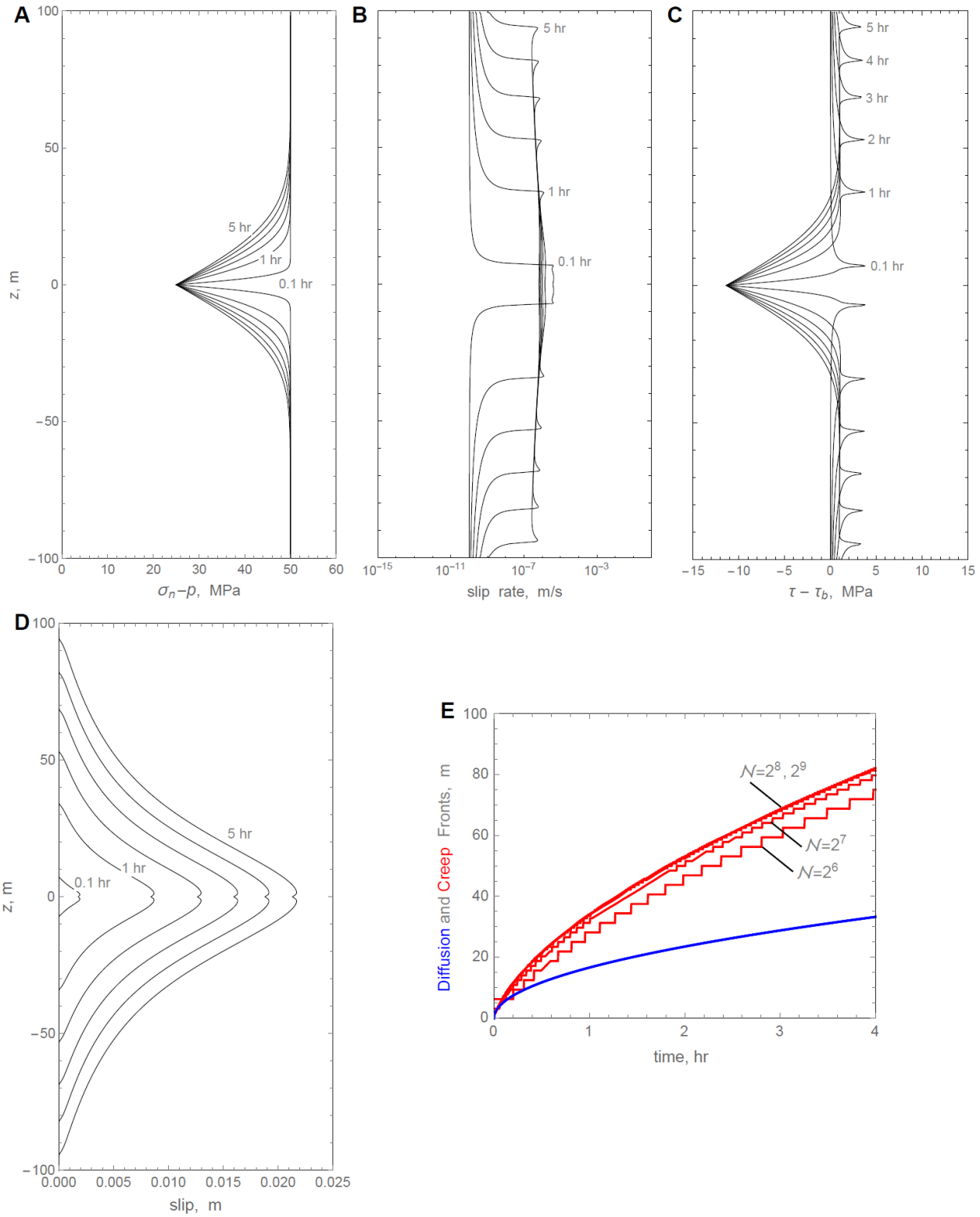

Fig. S8. Numerical example of accelerated creep on a frictionally stable fault with homogeneous properties driven by 1D pore pressure diffusion from a point source of constant overpressure. (N=29 grid points). (**A**) Effective normal stress. (**B**) Slip rate. (**C**) Change in shear stress. (**D**) Slip. All plotted at 0.1, 1, 2, …, 5 hours after the start of fluid injection. (**E**) Creep (red) and pore pressure diffusion (blue) fronts and the solution dependence on the spatial discretization (number of grid nodes N). The creep front is defined by the peak shear stress, (**C**), while the diffusion front corresponds to pore pressure change of 5% of the peak value, (**A**).

Table S1. Completions data for each stage. ISIP = Instantaneous shut-in pressure. Planned stages 27-30 were not completed due to seismicity exceeding the Alberta Energy Regulator Traffic Light Protocol (*40*).

Stage #	Start Time	Stop Time	Average Pressure (MPa)	Breakdown Pressure (MPa)	Maximum Pressure (MPa)	Estimated Closure Gradient (kPa/m)	ISIP (MPa)	Total Pumped Fluid (m^3)
1	1/4/2016 18:02	1/4/2016 20:47	68.1	45.0	74.1	19.75	45.8	1255.8
2	1/5/2016 4:13	1/5/2016 7:33	72.4	60.0	79.6	19.83	46.1	1350.0
3	1/5/2016 12:00	1/5/2016 14:56	70.6	50.2	75.1	20.08	47.1	1219.5
4	1/5/2016 20:35	1/5/2016 23:28	70.5	53.0	74.3	21.05	51.0	1305.2
5	1/6/2016 3:31	1/6/2016 6:30	72.7	53.2	78.4	20.75	49.8	1294.3
6	1/6/2016 10:21	1/6/2016 13:13	69.4	51.6	72.7	20.88	50.3	1303.6
7	1/6/2016 16:39	1/6/2016 19:50	67.0	50.1	70.4	19.65	45.4	1287.2
8	1/6/2016 23:19	1/7/2016 2:02	67.9	50.5	71.2	20.03	46.9	1252.0
9	1/7/2016 21:33	1/8/2016 0:25	68.6	50.1	73.0	20.43	48.5	1235.9
10	1/8/2016 3:34	1/8/2016 6:23	66.3	48.8	68.0	20.18	47.5	1236.1
11	1/8/2016 9:30	1/8/2016 12:23	66.8	47.4	74.6	19.58	45.1	1224.1
12	1/8/2016 15:30	1/8/2016 18:16	65.7	48.0	73.7	20.25	47.8	1205.7
13	1/8/2016 21:23	1/9/2016 0:00	64.0	49.7	66.4	20.23	47.7	1173.5
14	1/9/2016 2:55	1/9/2016 5:40	64.3	47.7	65.9	20.38	48.3	1204.8
15	1/9/2016 16:52	1/9/2016 20:14	65.2	47.7	70.7	20.43	48.5	1508.0
16	1/9/2016 23:31	1/10/2016 2:09	65.5	49.5	68.5	20.80	50.0	1179.1
17	1/10/2016 5:33	1/10/2016 8:20	64.3	48.7	69.3	20.55	49.0	1225.8
18	1/10/2016 11:02	1/10/2016 13:43	64.4	47.8	66.5	20.38	48.3	1173.9
19	1/10/2016 16:20	1/10/2016 19:05	63.0	46.5	65.5	20.08	47.1	1182.2
20	1/10/2016 21:47	1/11/2016 0:43	62.0	47.2	64.2	20.33	48.1	1163.0
21	1/11/2016 7:17	1/11/2016 9:55	61.3	46.8	64.7	20.08	47.1	1084.3
22	1/11/2016 12:25	1/11/2016 15:06	65.2	47.7	87.6	20.65	49.4	1175.3
23	1/11/2016 17:37	1/11/2016 20:18	62.5	49.5	75.9	20.78	49.9	1168.3
24	1/11/2016 22:45	1/12/2016 1:11	61.7	49.9	64.0	20.55	49.0	1087.3
25	1/12/2016 4:21	1/12/2016 6:55	60.8	48.8	63.1	20.35	48.2	1119.0
26	1/12/2016 9:53	1/12/2016 11:34	59.5	50.4	74.7	20.13	47.3	616.3